On the load-area relation in rough adhesive contacts

Khajeh Salehani, M.; van Dokkum, J. S.; Irani, N.; Nicola, L.

DOI
10.1016/j.triboint.2019.106099

Publication date
2020

Document Version
Final published version

Published in
Tribology International

Tribology International 144 (2020) 106099

Contents lists available at ScienceDirect

Tribology International

journal homepage: http://www.elsevier.com/locate/triboint

On the load-area relation in rough adhesive contacts

M. Khajeh Salehani [a], J.S. van Dokkum [a], N. Irani [a], L. Nicola [a,b,*]

[a] Department of Materials Science and Engineering, Delft University of Technology, the Netherlands
[b] Department of Industrial Engineering, University of Padua, Italy

ARTICLE INFO

Keywords:
Contact area and load
Self-affine roughness
Adhesion
Cohesive-zone model

ABSTRACT

It is well established that, at small loads, a linear relation exists between contact area and reduced pressure for elastic bodies with non-adhesive rough surfaces. In the case of adhesive contacts, however, there is not yet a general consensus on whether or not linearity still holds. In this work evidence is provided, through numerical simulations, that the relation is non-linear. The simulations here presented can accurately describe contact between self-affine adhesive rough surfaces, since they rely on Green's function molecular dynamics to describe elastic deformation and on coupled phenomenological traction-separation laws for the interfacial interactions. The analysis is performed for two-dimensional compressible and incompressible bodies under plane strain conditions. Interfaces with various roughness parameters and work of adhesion are considered.

1. Introduction

Our understanding of friction relies on Amonton's law, which states that the friction force is directly proportional to the applied normal load. The common interpretation of this law is that the friction force increases linearly with contact area, which in turn increases linearly with the applied normal load. For non-adhesive elastic rough surface contacts, state-of-the-art numerical simulations [1–8] have confirmed that there is indeed a linear relation between relative contact area and reduced pressure:

$$a_{\mathrm{rel}} = \kappa\left(\frac{p}{\overline{g}E^*}\right), \tag{1}$$

where p is the load divided by an arbitrary but fixed reference area, E^* is the effective contact modulus, and $\overline{g}$ is the root-mean-square gradient (RMSG) over the nominal contact area. The relationship holds true even for Hertzian indenters and for line contacts provided that the reduced pressure is defined as $p_{\mathrm{r}}^* := p/(\overline{g}_{\mathrm{r}}\, E^*)$ where $\overline{g}_{\mathrm{r}}$ is the RMSG over the real contact area, as demonstrated in Refs. [9,10]. Experiments performed on 3D printed rough surfaces seem to confirm the linear relationship [11,12].

Very recently, Weber et al. [13] succeeded in the endeavour of visualizing *in situ* the increase in contact area during the indentation of a glass surface by means of two transparent rough materials: polystyrene and polymethyl-methacrylate. They found that contact area does not increase linearly with the applied normal load. The reasons for the non-linearity in the experiment can be manyfold. In the literature two main possible causes for non-linearity have been identified: the plastic behaviour of materials [14], and the adhesive interaction between contacting surfaces [15,16]. Interestingly, recent numerical studies on plasticity, although confined to metals, showed again linear area-to-load curves, albeit with a different slope than elasticity [17,18].

Regarding adhesive contacts, there is not yet a general consensus on the linearity between contact area and normal load. Carbone et al. [19] studied contact between adhesive rough surfaces via numerical calculations, employing a boundary element method (BEM), and analytically, using an extended version of Persson's theory. They found that, even in the presence of adhesion, the contact area still linearly increases with the normal load. More recently, Rey et al. [20] obtained similar results using a fast Fourier transform based BEM algorithm. However, the results obtained by Pastewka and Robbins [15], using a Green's function technique, and by Violano and Afferrante [16], employing the Derjaguin-Muller-Toporov (DMT) model, show a non-linear relation between contact area and normal load. The differences observed in these works in the load–area relationship, namely linearity or non-linearity, is unlikely caused by a difference in the employed methodology, but most probably a consequence of the specific selection of roughness parameters and/or interfacial properties. To assess whether this hypothesis is correct, we will here perform a comprehensive study where roughness parameters, interfacial properties, and elastic properties are varied.

To this end, Green's function molecular dynamics (GFMD)

* Corresponding author. Department of Industrial Engineering, University of Padua, Italy.
E-mail address: l.nicola@tudelft.nl (L. Nicola).

https://doi.org/10.1016/j.triboint.2019.106099
Received 10 September 2019; Received in revised form 28 November 2019; Accepted 2 December 2019
Available online 13 December 2019

simulations are performed to model indentation of flat elastically deforming body indented by a rough rigid solid. The adhesive or frictional interactions between the surfaces is described through traction–separation laws. New insights are provided into the role of roughness parameters (root-mean-square height, Hurst exponent and small wavelengths), interfacial properties, and material parameters on the relation between contact area and normal load.

The strength of the simulations performed in the current work compared with previous studies lies in the way the interfacial interactions are treated. Thanks to the coupling between normal and tangential traction–separation laws, it is possible to properly track the evolution of the contact deformation also for solids with generic Poisson's ratio. Adhesion between surfaces implies that the lateral displacement of the deforming surface is partly constrained by tangential tractions. This constraint affects the way in which the contacting surfaces deform [21].

2. Problem definition and method of solution

A 1+1–D self-affine rough rigid body indents a flat elastic isotropic half-plane under plane strain conditions. The analysis is performed on an unit cell, periodic in x-direction (see Fig. 1). The interface is taken to be adhesive or non-adhesive.

The simulation starts with the surfaces being fully out of contact, their closest points being at a distance δ_0. This is necessary to capture the onset of contact between adhesive surfaces. A linearly increasing normal displacement U_z is then applied on the rigid indenter and the total tractions at the interface are calculated as a function of the penetration distance, defined as $\delta := U_z - \delta_0$. The elastic deformation of the elastic surface is calculated using the GFMD technique [7,21–24]. For each increment of the applied displacement, the equilibrium position of the surface nodes is calculated in reciprocal space using the damped energy minimization method [3] with the position Störmer-Verlet algorithm [25]. Since in Fourier space the displacement modes decouple, the modes can be damped independently, leading to a fast converging solution. The interactions between adhesive interfaces is controlled through cohesive-zone (CZ) constitutive laws that link the surface tractions $T_{\mathrm{cz,n}}$ and $T_{\mathrm{cz,t}}$ to the gap functions Δ_n and Δ_t, where the subscripts n and t refer to normal and tangential components. Following [26], the CZ laws are expressed as

$$T_{\mathrm{cz,n}} = \frac{\varphi_\mathrm{n}}{\delta_\mathrm{n}}\left(\frac{\Delta_\mathrm{n}}{\delta_\mathrm{n}}\right)\exp\left(-\frac{\Delta_\mathrm{n}}{\delta_\mathrm{n}}\right)\exp\left(-\frac{\Delta_\mathrm{t}^2}{\delta_\mathrm{t}^2}\right),$$
$$T_{\mathrm{cz,t}} = 2\frac{\varphi_\mathrm{t}}{\delta_\mathrm{t}}\left(\frac{\Delta_\mathrm{t}}{\delta_\mathrm{t}}\right)\exp\left(-\frac{\Delta_\mathrm{n}}{\delta_\mathrm{n}}\right)\exp\left(-\frac{\Delta_\mathrm{t}^2}{\delta_\mathrm{t}^2}\right). \tag{2}$$

Here, $(\varphi_\mathrm{n}, \varphi_\mathrm{t})$ are the works of separation and $(\delta_\mathrm{n}, \delta_\mathrm{t})$ are the characteristic lengths. Notice that for (nearly) incompressible solids subjected to pure normal loading, the relative tangential displacement of the surface nodes is negligible ($\Delta_\mathrm{t} \approx 0$), as discussed in Ref. [22]. For those cases, Eq. (2) reduces to

$$T_{\mathrm{cz,n}} = \frac{\varphi_\mathrm{n}}{\delta_\mathrm{n}}\left(\frac{\Delta_\mathrm{n}}{\delta_\mathrm{n}}\right)\exp\left(-\frac{\Delta_\mathrm{n}}{\delta_\mathrm{n}}\right). \tag{3}$$

In the case of non-adhesive contacts, where $T_{\mathrm{cz,t}} = 0$, the normal interfacial interaction is controlled by a hard-wall potential.

When the work of adhesion is zero, the real area of contact is defined as the area connecting nodes that interact with each other through compressive tractions larger than zero. When the work of adhesion is positive, the true contact area is taken to include also the surface under tension, and is therefore defined as the area where the normal tractions are smaller than a specified tolerance, chosen to be $\tilde{}0.001\ \ (\varphi_\mathrm{n}/\delta_\mathrm{n})$.

The surface of the rigid indenter is assumed to have a self-affine roughness with a Gaussian height distribution. The roughness is generated by means of the spectral method described in Ref. [27]. The power spectrum density function of the self-affine roughness $C(q)$, with q being the wave number, is given by

$$C(q) = C(q_\mathrm{r}) \times \begin{cases} 1 & \text{for} \quad \lambda_\mathrm{r} < \dfrac{2\pi}{q} \le \mathscr{L}; \\ \left(\dfrac{q}{q_\mathrm{r}}\right)^{-(1+2H)} & \text{for} \quad \lambda_{s,H} < \dfrac{2\pi}{q} \le \lambda_\mathrm{r}; \\ 0 & \text{for} \quad \lambda_s \le \dfrac{2\pi}{q} \le \lambda_{\mathrm{s,H}}, \end{cases} \tag{4}$$

where $C(q_\mathrm{r})$ is a scaling pre-factor and the fractal dimension is $D_\mathrm{f} = 2 - H$, with H being the Hurst exponent [19]. Here, λ_r is the roll-off wavelength, $\mathscr{L}$ is the longest wavelength and equal to the width of the periodic unit cell, $\lambda_{\mathrm{s,H}}$ is the roll-on wavelength, and λ_s is the smallest wavelength.

The RMSG over the real contact area $\overline{g}_\mathrm{r}$ is calculated numerically as

$$\overline{g}_\mathrm{r} = \sqrt{\frac{\sum_{i=1}^{n} g_i^2}{n}}, \tag{5}$$

where n is the total number of contact points and g_i^2 is the local mean-square gradient at point i which is obtained as

$$g_i^2 = \frac{1}{2}\left[\left(\frac{h_i - h_{i+1}}{l}\right)^2 + \left(\frac{h_i - h_{i-1}}{l}\right)^2\right], \tag{6}$$

with h_i being the height profile of the indenter at point i and l is the spacing between the surface nodes.

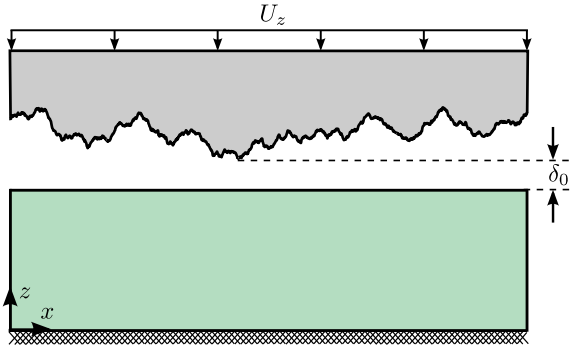

Fig. 1. Sketch of the analysed 1 + 1 – dimensional contact problem: a rigid body with self-affine rough profile indents a flat elastic body. The simulation starts when the surfaces are well out of contact and traction is negligible.

2.1. Choice of parameters

The deformable solid is elastic isotropic with elastic modulus 70 GPa and Poisson's ratio ranging from $\nu = 0.1$ to 0.45. Compared to the solid, the indenter is rigid, with $E_\mathrm{i} = 1000\ \ E$. The dimensionless normal work of separation, $\varphi_\mathrm{n}^* = \varphi_\mathrm{n}/(\delta_\mathrm{n}E)$ and tangential work of separation, $\varphi_\mathrm{t}^* = \varphi_\mathrm{t}/(\delta_\mathrm{t}E)$ are taken to range from 0.001 to 0.15, i.e. from weak adhesion as typical of metals, to strong adhesion as typical of bio-adhesives. The tangential-to-normal work of separation is $c = \varphi_\mathrm{t}^*/\varphi_\mathrm{n}^*$. The effect of friction is studied by considering two values for the tangential-to-normal work of separation $c = \varphi_\mathrm{t}^*/\varphi_\mathrm{n}^*$: $c = 0$ for frictionless contacts and $c = 0.5$ for highly frictional contacts [22].

Simulations are carried out for Hurst exponents $H = 0.2, 0.5, 0.8$ and root-mean-square heights (RMSHs) $h_\mathrm{rms} = 10, 15, 30$ nm. Convergence of the results is guaranteed by selecting $\varepsilon_\mathrm{t} = \lambda_\mathrm{r}/\mathscr{L} = 8^{-1}$ [10,28] and $\varepsilon_\mathrm{c} = \lambda_\mathrm{s}/\lambda_{\mathrm{s,H}} = 32^{-1}$. The fractal discretization, which defines the number of wavelengths used to describe the rough profile, is chosen to be

$\varepsilon_f = \lambda_{s,H}/\lambda_r = 512^{-1}$, and the role of the small wavelengths on the load-area relation is assessed for $\varepsilon_f = 128^{-1}$ and 64^{-1}. This is performed by keeping λ_r constant and for $\lambda_{s,H} = 2.5, 10, 20$ nm.

To account for the random nature of the roughness, numerical calculations are performed for 10 different randomly generated rough profiles for any combination of H, h_{rms}, and ε_f. Thereafter, the average across realization is taken over the obtained numerical results.

3. Non-adhesive contacts

First, simulations are performed for non-adhesive contacts. Rigid rough indenters with Hurst exponents $H = 0.2, 0.8$ and RMSH $h_{rms} = 10, 30$ nm indent an elastic solid with elastic modulus $E = 70$ GPa and Poisson's ratio $\nu = 0.45$ and $\nu = 0.1$.

The curves for relative contact area a_{rel} versus reduced pressure $p_r^* := p/(\bar{g}_r E^*)$ in Fig. 2 are independent of both the compressibility of the solid and the roughness parameters considered. Furthermore, Fig. 2 confirms that a_{rel} increases linearly with p_r^* in all cases. We find the proportionality factor ~1.75. This is in line with the findings in Ref. [10] for incompressible solids. In the following section, it is shown how adhesion affects the dependence of the relative contact area on the reduced pressure.

4. Adhesive contacts

In Fig. 3 the load-area response obtained in the previous section for non-adhesive contacts is contrasted with the response of adhesive contacts with various normal works of separation φ_n^*. The deformable solid is here assumed to be nearly incompressible $\nu = 0.45$ and hence, the cohesive law has only normal components (see Eq. (3)).

The contact area is defined as the sum of the portions of interface where there is an interaction between surfaces, i.e., repulsive and/or attractive normal tractions, within the specified tolerance. As expected, for the same load, the contact area of adhesive contacts is larger than that of non-adhesive contacts. More interesting is that, in adhesive contacts, the linearity between a_{rel} and $p_r^* = p/(E^*\bar{g}_r)$ breaks down: at small loads contact area increases faster with adhesion, at larger loads the increase is less pronounced. Notice that the traction-separation law at the interface introduces a characteristic length in addition to the lengths that describe the surface roughness. Figure 3b is a zoom-in of Fig. 3a at small loads, which allows the reader to see that for adhesive contacts the contact area is larger than zero also for negative approach

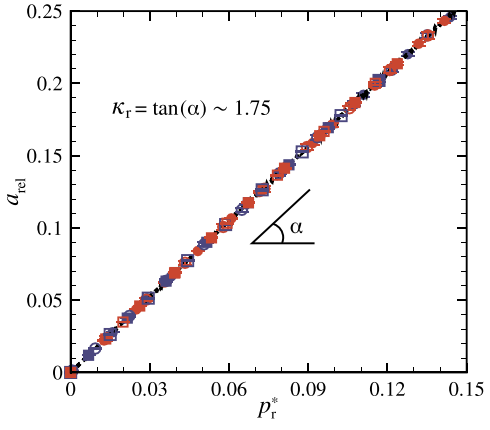

Fig. 2. Non-adhesive contacts: relative contact area a_{rel} versus reduced pressure p_r^*. The results are shown for Hurst exponent $H = 0.2$ (squares) and $H = 0.8$ (circles), and Poisson's ratio $\nu = 0.45$ (red) and $\nu = 0.1$ (blue). Closed and open symbols are for RMSG $h_{rms} = 10$ nm and $h_{rms} = 30$ nm, respectively. Note that error bars are smaller than the symbols. (For interpretation of the references to colours in this figure, the reader is referred to the Web version of this article.)

displacement.

For a better understanding of the differences between adhesive and non-adhesive contacts, we present separately in Fig. 4 the increase of p/E^*, a_{rel}, $\bar{g}_r/\bar{g}$ as a function of the penetration distance δ.

Figure 4a shows that the difference in p^* versus δ curves of adhesive (various φ_n^*) and non-adhesive contacts is negligible even at a very small contact pressure. At the onset of contact, the curves for more adhesive interfaces are slightly lower than those for less adhesive interfaces. With increasing the loading, the difference vanishes, because, apparently, the attractive tractions are compensated by additional repulsive tractions that generate during loading on the contacts. A large difference between adhesive and non-adhesive contacts is instead found in how the relative contact area a_{rel} increases with penetration distance (see Fig. 4b). As to be expected, the larger is adhesion, the more the surfaces conform.

For non-adhesive contacts, normalizing p^* with the RMSG calculated on the real contact area, $\bar{g}_r$, leads to a linear relationship between load and area [10]. For adhesive contacts, normalizing p^* with $\bar{g}_r$ will have no such effect, since $\bar{g}_r$ is practically just a constant as can be evinced by looking at Fig. 4b. Here, $\bar{g}_r$ is normalized on the constant $\bar{g}$. Note that, while the normal work of separations varies, the ten realizations of the rough profile Fig. 4a–c have the same roughness and therefore $\bar{g}$. For all adhesive contacts considered in this section, $\bar{g}_r/\bar{g} \to 1$ at very small penetration distance. This also means that for adhesive contacts it is pointless to distinguish between $\bar{g}_r$ and $\bar{g}$ for the roughnesses considered here.

As demonstrated in Fig. 4b, the larger the adhesive forces, the better the deformable solids conforms to the rough rigid profile, even to the finer features of the roughness. This can be better seen in Fig. 5 which gives a snapshot, i.e. one out of the ten realizations, of the interface at $\delta = 20$ nm, for the cases shown in Fig. 4. With more adhesion, at the same penetration distance a larger number of roughness peaks gets into contact. Given that the small roughness differs locally quite significantly between realizations, the error bars become larger with adhesion, as one can see in Fig. 4b.

In the subsequent sections we will focus on highlighting the effect of roughness parameters on adhesion.

4.1. Effect of roughness parameters

It is well known that for non-adhesive contacts the area-load relationship is not only linear but also independent of h_{rms} and H if the pressure is normalized on the RMSG ($\bar{g}$ for surface contacts and $\bar{g}_r$ for line contacts). Figure. 6 demonstrates that this is not the case for adhesive contacts. The simulations are performed for a solid with Poisson's ratio $\nu = 0.45$, an adhesive surface with normal work of separation $\varphi_n^* = 0.15$ and contrasted with the line for non-adhesive contacts. The deviation of the adhesive curves from the line representing non-adhesion, gives the effect of adhesion. The following observations can be made: (1) when adhesive rough surfaces differ only by RMSH, (Fig. 6a), the smaller the h_{rms} the larger the relative contact area at a given reduced pressure p_r^*; (2) the smaller the h_{rms} the 'more pronounced' is non-linearity. The effect of adhesion increases with decreasing RMSH. This is to be expected, since for smaller RMSH the gap decreases. The effect of Hurst exponent on adhesion presented in Fig. 6b, is less neat: it is weakest for the smallest Hurst exponents considered, where the RMSG is large, and therefore is more difficult to form large patches of contact. In our simulations, however, it is the surface with Hurst exponent $H = 0.5$ that displays the strongest effect of adhesion while plotting $a_{rel} - p_r^*$. It is noteworthy that non-linearity increases with increasing Hurst exponent and that the spread of the simulations also increases with it, given that the number of contacts in a unit cell decreases with H.

Next, we proceed to investigate how the contact behaviour depends on the finest roughness features. Simulations are performed for rough profiles with fractal discretizations $\varepsilon_f = 512^{-1}, 128^{-1}$, and 64^{-1}. The a_{rel} versus $p^*(= p/E)$ curves are presented in Fig. 7a, for Hurst exponents

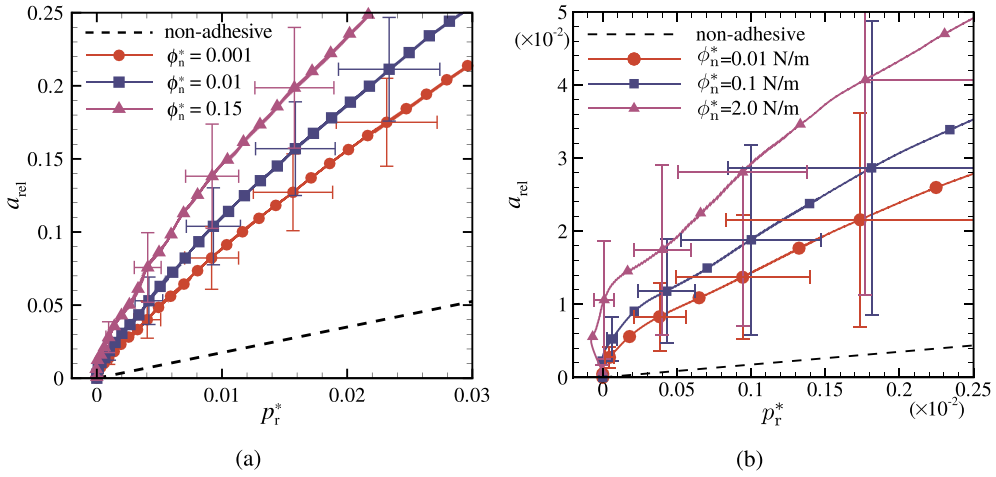

Fig. 3. (a) Relative contact area a_{rel} versus reduced pressure p_r^* for various normal works of separation φ_n^*. Dashed black line with the slope ~ 1.75 corresponds to the non-adhesive contact. The roughness parameters $H = 0.8$ and $h_{rms} = 10$ nm in all cases. For clarity only a selection of data points is shown. (b) A zoom-in of the figure at small loads.

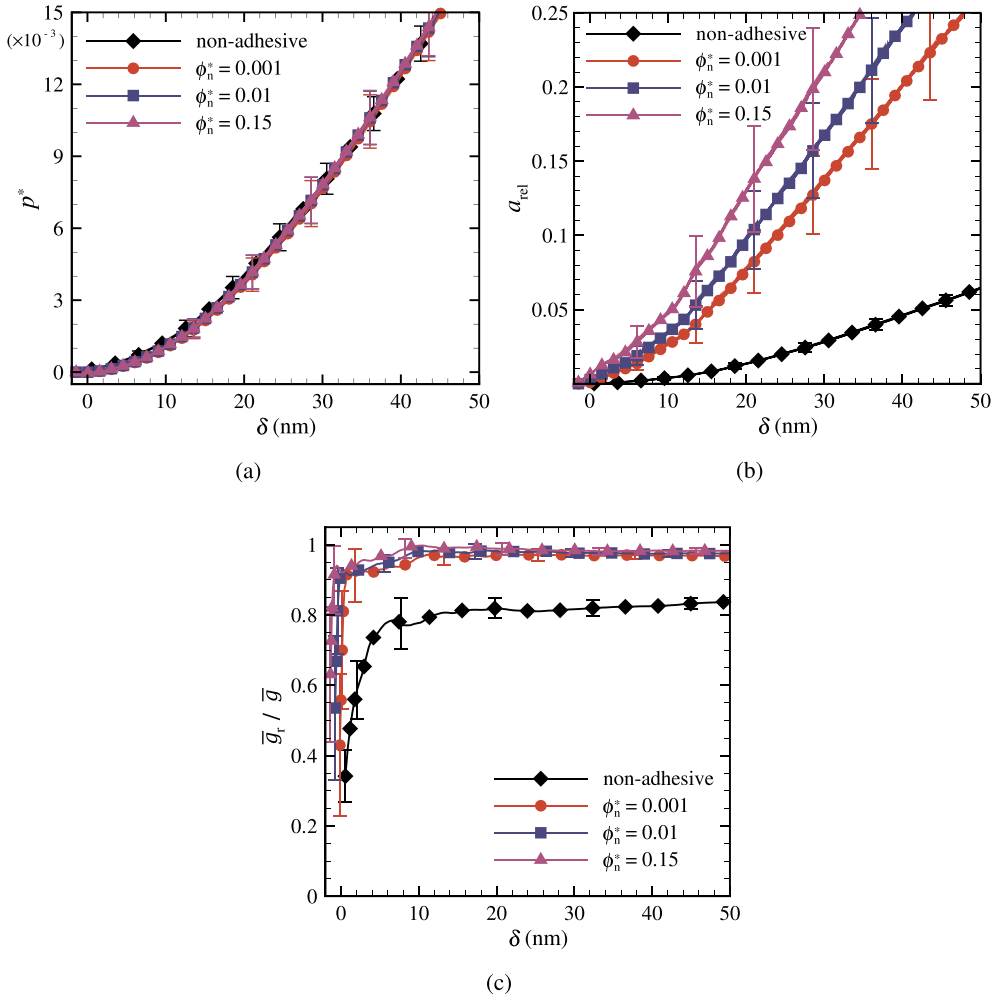

Fig. 4. (a) Normalized pressure p^*, (b) relative contact area a_{rel} versus penetration distance δ, and (c) normalized root-mean-square gradient $\overline{g}_r / \overline{g}$. The results are shown for various normal works of separation φ_n^* (the same considered in Fig. 3). The roughness parameters are $H = 0.8$ and $h_{rms} = 10$ nm.

$H = 0.8$ and 0.2.

For $H = 0.8$, the $a_{rel} - p^*$ curve is independent of ε_f, in line with the work by Violano et al. [29]. On the contrary, for $H = 0.2$, the contact behaviour becomes strongly dependent on the smaller wavelengths: the contact area increases with increasing ε_f. This is because when the surface does not contain the smaller wavelengths the surface becomes smoother and hence, adheres better to the substrate, as can be seen from the snapshots in Fig. 7b.

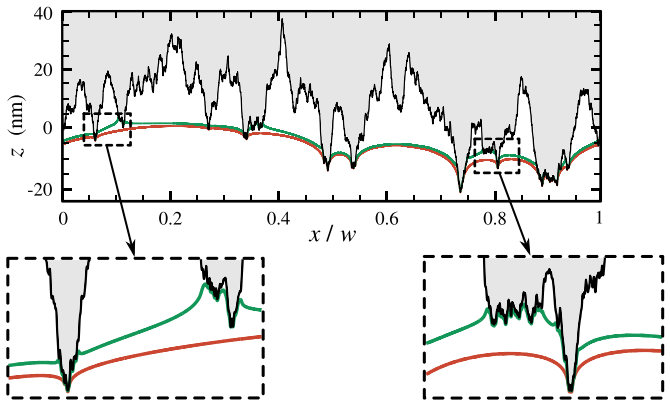

Fig. 5. A snapshot of the interface at the penetration distance $\delta = 20$ nm. The results correspond to the cases shown in Fig. 4. The indenter is gray and the surface profiles of the adhesive ($\varphi_n^* = 0.15$) and non-adhesive contacts are green and red, respectively. (For interpretation of the references to colours in this figure, the reader is referred to the Web version of this article.)

4.2. Effect of compressibility and friction

Finally, the roles of compressibility and of friction on the load-area relation are studied. Here, friction is included through the tangential work of separation φ_t^*. The interface interactions are defined by the two cohesive laws in Eq. (2).

Fig. 8 shows the results for Poisson's ratio ν ranging from 0.1 to 0.45. This figure demonstrates that the $a_{rel} - p^*$ relation is negligibly affected by the compressibility of the solid and frictional properties of the interface.

This is in line with the author's findings in Ref. [22], where a solid was indented by an array of circular punches: when contacts were closely spaced the lateral displacement of the surface nodes were negligible, due to the interference of the displacement fields of the neighbouring punches.

5. Concluding remarks

The role of adhesion on the load-area relation in elastic contact problems is studied. Simulations are performed using the Green's function molecular dynamics (GFMD) technique for the contact between

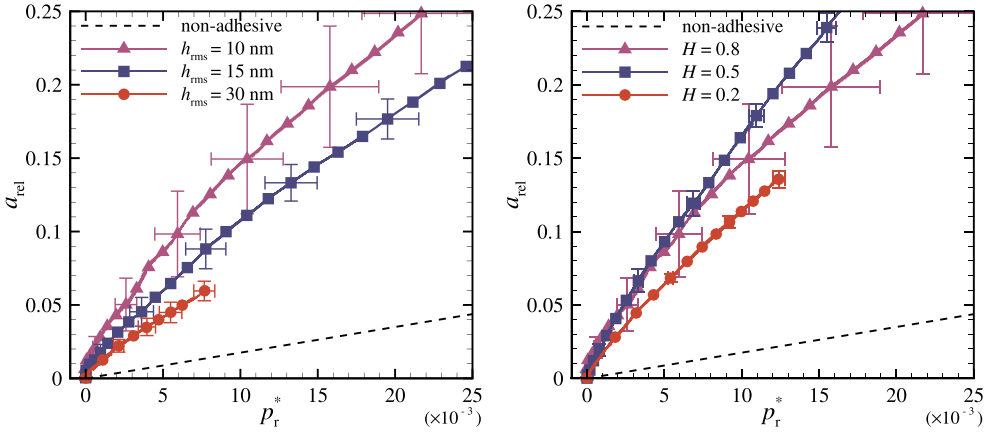

(a) $H = 0.8$ (b) $h_{rms} = 10$ nm

Fig. 6. Relative contact area a_{rel} versus reduced pressure p_r^* for rough adhesive contacts with various values of (a) root-mean-square height h_{rms} and (b) Hurst exponent H. The results are shown for the normal work of separation $\varphi_n^* = 0.15$.

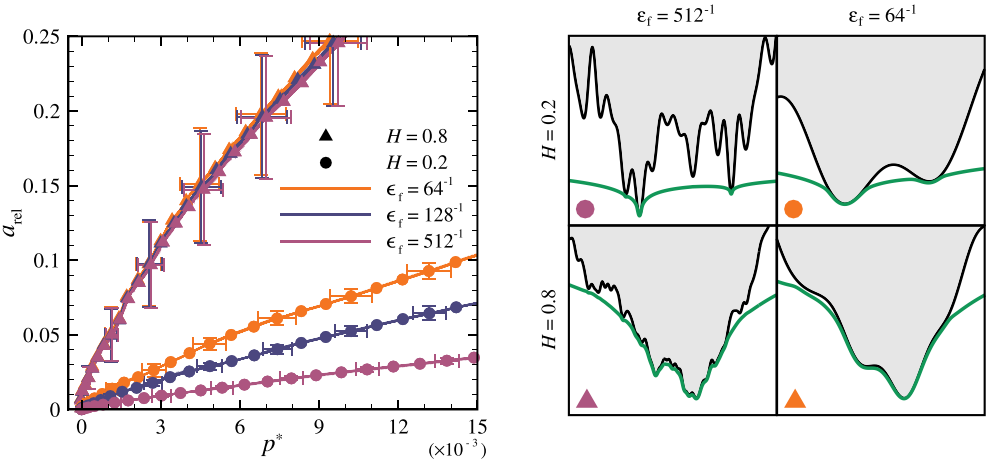

(a) (b)

Fig. 7. (a) Relative contact area a_{rel} versus normalized pressure p^* for various values of fractal discretization ε_f and Hurst exponent H. (b) Snapshots of a part of the interface for rough profiles with $\varepsilon_f = 512^{-1}, 64^{-1}$ and Hurst exponents $H = 0.8, 0.2$. In all cases, the root-mean-square height $h_{rms} = 10$ nm and the normal work of separation $\varphi_n^* = 0.15$.

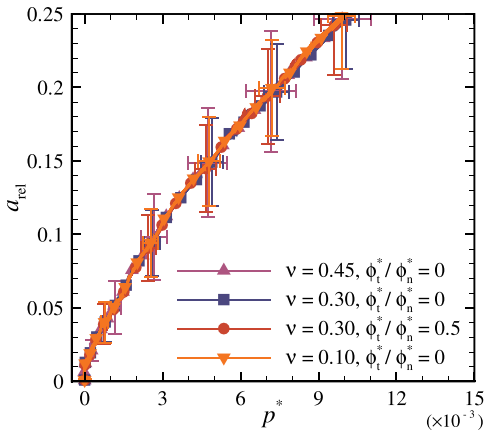

Fig. 8. Relative contact area a_{rel} versus normalized pressure p^* for random rough profile adhesive contacts. The results are shown for solids with various Poisson's ratios ν and interface friction properties. Friction is increased by increasing the tangential-to-normal work of separation $c = \varphi_t^*/\varphi_n^*$. The normal work of separation $\varphi_n^* = 0.15$, and the roughness parameters $H = 0.8$ and $h_{rms} = 10$ nm.

a self-affine rough rigid surface and an initially flat deformable solid. The interfacial interactions are modelled using coupled traction-separation laws. It is confirmed that the contact area of non-adhesive contacts linearly increases with reduced pressure, independently of Hurst exponent and root-mean-square height.

In the presence of adhesion, some key features are observed, as listed below.

- The load-area relation, $a_{rel} - p_r^*$, is non-linear. Deviation from linearity increases with the work of adhesion.
- Increasing the work of adhesion of a rough surface has negligible effect on the total load acting on the interface at a given penetration distance, but leads to an increase in contact area.
- The load-area relation, $a_{rel} - p_r^*$, depends on Hurst exponent and root-mean-square height.
- Non-linearity is more pronounced for rough profiles with large Hurst exponent and/or small root-mean-square height.
- The effect of adhesion is smaller for surfaces with large root-mean-square heights and/or small Hurst exponents.
- For small Hurst exponents the load-area relation depends on the small wavelengths cut-off used to described the roughness. In this case, non-linearity increases with increasing the small wavelength cut-off.
- Compressibility and friction can be neglected when investigating the load-area relation, since they affect it negligibly. This also entails that there is no need to use coupled cohesive-zone laws if one is only interested in the normal loading of rough surfaces: a traction-separation law in normal direction will suffice.

We speculate that simulations in previous literature showing linearity between contact area and load for adhesive contacts focused on surfaces with small Hurst exponent and/or large root-mean-square height. This is why non-linearity might have appeared as marginal, as well as the effect of the small wavelength cut-off.

CRediT author statement

Mohsen Khajeh Salehani: Conceptualization, Software, Data Analysis, Data Curation, Investigation, Writing-Original Draft Jan Steven van Dokkum: Conceptualization, Software, Data Analysis, Data Curation, Investigation Nilgoon Irani: Conceptualization, Supervision, Writing-Review & Editing Lucia Nicola: Conceptualization, Supervision, Writing-Review & Editing, Funding acquisition.

Declaration of competing interest

The authors declare that they have no known competing financial interests or personal relationships that could have appeared to influence the work reported in this paper.

Acknowledgement

LN received funding from the European Research Council (ERC) under the European Union's Horizon 2020 research and innovation programme (grant agreement no. 681813). LN also acknowledges support by the Netherlands Organisation for Scientific Research NWO and Dutch Technology Foundation STW (VIDI grant 12669).

References

[1] Persson BN. Theory of rubber friction and contact mechanics. J Chem Phys 2001;115(8):3840–61.
[2] Hyun S, Pei L, Molinari J-F, Robbins MO. Finite-element analysis of contact between elastic self-affine surfaces. Phys. Rev. E 2004;70(2):026117.
[3] Campañá C, Müser MH. "Contact mechanics of real vs. randomly rough surfaces: a Green's function molecular dynamics study. Europhys Lett 2007;77(3):38005.
[4] Carbone G, Bottiglione F. Asperity contact theories: do they predict linearity between contact area and load? J Mech Phys Solids 2008;56(8):2555–72.
[5] Yang C, Persson B. Contact mechanics: contact area and interfacial separation from small contact to full contact. J Phys Condens Matter 2008;20(21):215214.
[6] Putignano C, Afferrante L, Carbone G, Demelio G. The influence of the statistical properties of self-affine surfaces in elastic contacts: a numerical investigation. J Mech Phys Solids 2012;60(5):973–82.
[7] Prodanov N, Dapp WB, Müser MH. On the contact area and mean gap of rough, elastic contacts: dimensional analysis, numerical corrections, and reference data. Tribol Lett 2014;53(2):433–48.
[8] McGhee AJ, Pitenis AA, Bennett AI, Harris KL, Schulze KD, Urueña JM, Ifju PG, Angelini TE, Müser MH, Sawyer WG. Contact and deformation of randomly rough surfaces with varying root-mean-square gradient. Tribol Lett 2017;65(4):157.
[9] Müser MH. On the linearity of contact area and reduced pressure. Tribol Lett 2017;65(4):129.
[10] van Dokkum JS, Khajeh Salehani M, Irani N, Nicola L. On the proportionality between area and load in line contacts. Tribol Lett 2018;66(3):115.
[11] Bartolome L, Tato W. Experimental and numerical analysis of indentation on a thermoplastic polyurethane elastomer under cyclic loading. In: European conference; 8th, Constitutive models for rubber. CRC Press; 2013. p. 649–56.
[12] Borovsky B, Krim J, Syed Asif S, Wahl K. Measuring nanomechanical properties of a dynamic contact using an indenter probe and quartz crystal microbalance. J Appl Phys 2001;90(12):6391–6.
[13] Weber B, Suhina T, Junge T, Pastewka L, Brouwer A, Bonn D. "Molecular probes reveal deviations from Amontons' law in multi-asperity frictional contacts. Nat Commun 2018;9(1):888.
[14] Bak FS, Trzepieciński T, Bosiakov S, Rogosin S. Strain hardening effect on elastic-plastic contact of a rigid sphere against a deformable flat. In: *Advances in* mechanics: theoretical, computational and interdisciplinary issues: proceedings of the 3rd polish congress of mechanics (PCM) and 21st international conference on computer methods in mechanics (CMM), vol. 549. Gdansk, Poland: CRC Press; 2016. p. 77. 8-11 September 2015.
[15] Pastewka L, Robbins MO. Contact between rough surfaces and a criterion for macroscopic adhesion. Proc Natl Acad Sci 2014;111(9):3298–303.
[16] Violano G, Afferrante L. On DMT methods to calculate adhesion in rough contacts. Tribol Int 2019;130:36–42.
[17] Pei L, Hyun S, Molinari J, Robbins MO. Finite element modeling of elasto-plastic contact between rough surfaces. J Mech Phys Solids 2005;53(11):2385–409.
[18] Venugopalan SP, Nicola L. Indentation of a plastically deforming metal crystal with a self-affine rigid surface: a dislocation dynamics study. Acta Mater 2019;165:709–21.
[19] Carbone G, Scaraggi M, Tartaglino U. Adhesive contact of rough surfaces: comparison between numerical calculations and analytical theories. Eur Phys. J. E 2009;30(1):65.
[20] Rey V, Anciaux G, Molinari J-F. Normal adhesive contact on rough surfaces: efficient algorithm for FFT-based BEM resolution. Comput Mech 2017;60(1):69–81.
[21] Campañá C, Müser MH. Practical Green's function approach to the simulation of elastic semi-infinite solids. Phys Rev B 2006;74(7):075420.
[22] Khajeh Salehani M, Irani N, Müser M, Nicola L. Modelling coupled normal and tangential tractions in adhesive contacts. Tribol Int 2018;124:93–101.
[23] Venugopalan SP, Müser MH, Nicola L. Green's function molecular dynamics meets discrete dislocation plasticity. Model Simul Mater Sci Eng 2017;25(6):065018.
[24] Venugopalan SP, Nicola L, Müser MH. Green's function molecular dynamics: including finite heights, shear, and body fields. Model Simul Mater Sci Eng 2017;25(3):034001.
[25] Verlet L. "Computer" experiments" on classical fluids. i. thermodynamical properties of Lennard-Jones molecules. Phys Rev 1967;159(1):98.

[26] McGarry JP, Máirtín ÉÓ, Parry G, Beltz GE. Potential-based and non-potential-based cohesive zone formulations under mixed-mode separation and over-closure. part I: theoretical analysis. J Mech Phys Solids 2014;63:336–62.
[27] Müser MH, Dapp WB, Bugnicourt R, Sainsot P, Lesaffre N, Lubrecht TA, Persson BN, Harris K, Bennett A, Schulze K, et al. Meeting the contact-mechanics challenge. Tribol Lett 2017;65(4):118.
[28] Yastrebov VA, Anciaux G, Molinari J-F. From infinitesimal to full contact between rough surfaces: evolution of the contact area. Int J Solids Struct 2015;52:83–102.
[29] Violano G, Afferrante L, Papangelo A, Ciavarella M. On stickiness of multiscale randomly rough surfaces. 2018. arXiv:1810.10960.